

Optics Letters

Ultra-wideband and high-gain parametric amplification in telecom wavelengths with an optimally mode-matched PPLN waveguide

YONG MENG Sua, 1,2,* D JIA-YANG CHEN, 1,2 AND YU-PING HUANG 1,2

¹Department of Physics, Stevens Institute of Technology, 1 Castle Point Terrace, Hoboken, New Jersey 07030, USA ²Center for Quantum Science and Engineering, Stevens Institute of Technology, 1 Castle Point Terrace, Hoboken, New Jersey 07030, USA *Corresponding author: ysua@stevens.edu

Received 9 April 2018; revised 19 May 2018; accepted 21 May 2018; posted 23 May 2018 (Doc. ID 327999); published 15 June 2018

We report a wideband optical parametric amplification (OPA) over 14 THz covering telecom S, C, and L bands with observed maximum parametric gain of 38.3 dB. The OPA is realized through cascaded second-harmonic generation and difference-frequency generation (cSHG-DFG) in a 2 cm periodically poled LiNbO₃ (PPLN) waveguide. With tailored cross section geometry, the waveguide is optimally mode matched for efficient cascaded nonlinear wave mixing. We also identify and study the effect of competing nonlinear processes in this cSHG-DFG configuration. © 2018 Optical Society of America

OCIS codes: (190.4410) Nonlinear optics, parametric processes; (230.7370) Waveguides; (230.7405) Wavelength conversion devices; (130.3730) Lithium niobate.

https://doi.org/10.1364/OL.43.002965

Large-scale and pervasive deployment of mobile devices, along with communication technological advancement, has led to numerous bandwidth intensive applications, such as Internet of Things (IoT), cloud computing and storage, high-definition video broadcasting and sharing, etc. [1]. This has created increasing demand for higher capacity network infrastructure with larger transmission bandwidth and faster signal processing [2]. Wavelength-division multiplexing (WDM) within the amplification bandwidth of an erbium-doped fiber amplifier (EDFA), along with high-speed electro-optic modulation and coherent detection schemes, has improved the bandwidth and spectral efficiency, thereby adequately addressing the growth of telecommunication traffic over the last decade [3,4]. Nonetheless, a continuous surge in optical communication traffic has motivated numerous efforts in boosting its capacity, most notably by space-division multiplexing [5], hybrid-distributed Raman-EDFA amplification [6], and broadband optical parametric amplification (OPA) [7].

Implemented through second- (χ^2) and third-order (χ^3) optical nonlinearities, OPA has shown the potential to significantly increase present optical communication capacity by providing broadband gain at arbitrary wavelengths beyond

WDM transmission systems. Advantageously, optical nonlinearities possess femtosecond response time, thus allowing ultrafast all-optical signal processing [4,8]. Lately, χ^2 -based OPA in periodically poled lithium niobate (PPLN) waveguides has drawn attention as an appealing option for broadband optical signal amplification and processing for telecom network systems [9-11]. Apparently, cascaded second-harmonic generation and difference-frequency generation (cSHG-DFG) configuration on one PPLN waveguide, which requires only a single telecom pump, is compact and highly compatible with current optical network infrastructure [9,10]. In addition, with typically short interaction length, the χ^2 -based OPA is advantageous in suppressing optical signal degradation arising from competing nonlinear phenomena, such as stimulated Brillouin scattering and cross- and self-phase modulations. Despite the plausible gain demonstrated recently by cSHG-DFG OPA in PPLN, its gain bandwidth is still fairly limited, with fundamental limitations posed by undesirable competing nonlinear processes and spontaneous parametric fluorescence, which restrict its uses in classical optical communications [9,10] and quantum information processing [12].

In this Letter, we demonstrate wideband parametric amplification covering *S*, *C*, and *L* telecom bands by using an optimally mode-matched PPLN waveguide with the cSHG-DFG configuration driven by a single telecom pump. The amplification bandwidth is at least 14 THz, as it is currently limited by the accessible wavelength range of the signal. With pump peak power of 41 dBm at 1550.6 nm, we observe maximum parametric amplification of 38 dB. To the best of our knowledge, these values represent the largest bandwidth and the highest gain among reported results based on cSHG-DFG OPA [10,13]. In parallel, we identify the competing nonlinear optical processes and intrinsic noise of this cSHG-DFG OPA, which are crucial for applications in all-optical signal processing and communications.

For the single-pump cSHG-DFG operation, two distinct nonlinear processes are involved, which are SHG and DFG, as illustrated in Fig. 1(a). For a quasi-phase-matched (QPM) PPLN waveguide, SHG and DFG are efficient only when the interacting optical waves satisfy the energy and momentum conservations (phase matching), given as

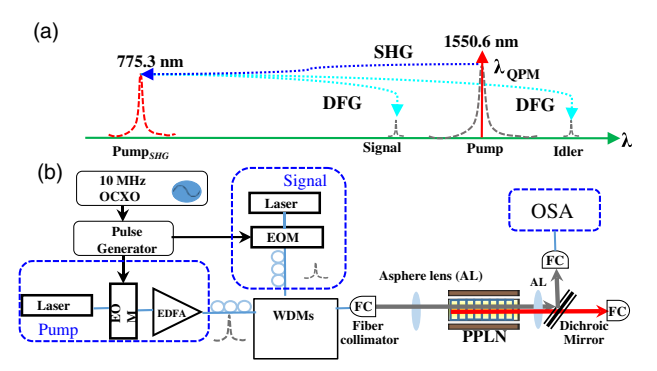


Fig. 1. (a) Illustration of cSHG-DFG processes for OPA. (b) Experimental setup for OPA.

$$2k_p - k_{\rm SH} - \frac{2\pi}{\Lambda} = 0, \qquad 2\omega_p = \omega_{\rm SH}, \tag{1}$$

$$k_{\mathrm{SH}} - k_{\mathrm{s}} - k_{i} - \frac{2\pi}{\Lambda} = 0,$$
 $\omega_{\mathrm{SH}} + \omega_{\mathrm{s}} = 2\omega_{\mathrm{s}} + \omega_{i}.$ (2)

Here, $k_j = n_{\rm eff}(\omega_j, T)\omega_j/c$ $(j = {\rm SH}, p, s, i)$ is the wavenumber for the SH, pump, signal, and idler, respectively, with n and ω_j being each one's effective refractive index and angular frequency. T and Λ are the temperature and periodic poling period of the PPLN. By using the temperature-dependent generalized Sellmeier equation [14] and a numerical mode solver to obtain $n_{\rm eff}$, we find that $k_s + k_i \approx 2k_p$ within the bandwidth of interest, so that the required Λ is approximately the same for both SHG and DFG. For the current waveguide temperature stabilized at 26.8 ± 0.1 °C, Λ is $17.2 \ \mu m$ with a duty cycle of 50%, for wavelengths $\approx 1550 \ nm$. As described in Eqs. (1) and (2), only a single pump is needed to produce SHG, which will act as the pump for the successive DFG process, where the signal is amplified and a phase-conjugate idler is produced.

We utilize a 2-cm-long commercial PPLN ridge waveguide made from a Y-cut LiNbO₃ substrate (5-mol.% Mg-doped) with 5 μm LN layer on top of 2 μm silicon dioxide (SiO₂) [Fig. 2(a)]. To achieve the optimum mode overlap between all interacting waves, the core of the PPLN waveguide is etched on the LN layer with 6 µm channel width and 2.4 µm depth. A high-precision ($\pm 0.02 \mu m$) dry etching technique ensures that the fabrication variation is well below the design tolerance of $\pm 0.2 \ \mu m$ for optimal mode matching. The waveguide is overcladded by a 5 µm layer of SiO₂ for phase matching, as depicted in Fig. 2(a). The modes of SHG and pump light are shown in Figs. 2(c) and 2(d), captured by using a high NA (0.45) aspheric lens with CMOS and IR cameras, respectively. Figures 2(e) and 2(f) show the quasi-transverse-electric (quasi-TE) modes for the SH (775.3 nm) and pump (1550.6 nm) light, which are simulated via the finite element method (FEM) based on the actual waveguide parameters. As seen, the two modes are nearly identical, which is attributed to the carefully chosen width and depth of the etched waveguide. Furthermore, the simulated quasi-TE modes ranging from 1450 to 1650 nm (not shown) are found to be very similar to the pump mode shown in Fig. 2(f). This excellent mode overlap of the interacting waves in the PPLN is crucial for attaining high gain and broadband in OPA, where the internal efficiency of both QPM SHG and DFG in the PPLN waveguide is limited by the spatial mode overlap, given as [15]

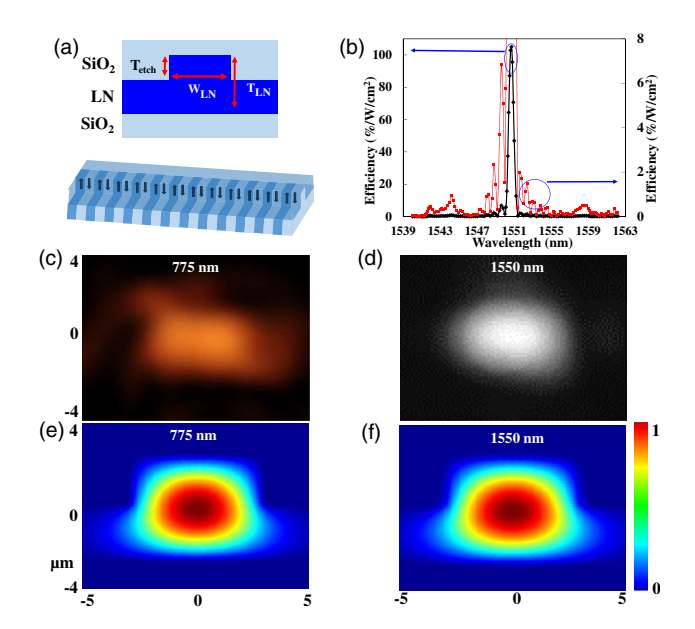


Fig. 2. (a) Schematic illustrating (top) cross sectional dimensions and (bottom) uniform poling profile of PPLN waveguide. $W_{\rm LN}=6~\mu{\rm m},~T_{\rm etch}=2.4~\mu{\rm m},~T_{\rm LN}=5~\mu{\rm m};$ (b) phase matching profile in black color with red color is the 12.5-times scaled-up plot; measured spatial mode profiles of (c) generated SHG (color) and (d) pump (grayscale); corresponding simulated quasi-TE spatial modes at wavelength of (e) 775 nm and (f) 1550 nm.

$$\eta_{\text{norm}} \propto \frac{\iint E_{2\omega}^* E_{\omega}^2 dy dz}{\sqrt{\iint |E_{2\omega}|^2 dy dz} \iint |E_{\omega}|^2 dy dz}.$$
(3)

First, we measure the SHG phase matching profile of the PPLN waveguide at 26.8°C in the undepleted pump regime. A wavelength-tunable laser with narrow linewidth is coupled from a single-mode fiber (SMF) collimator into the antireflection-coated PPLN waveguide along TE polarization by using an aspheric lens with coupling loss ≈1.1 dB. The measured SH power as the wavelength is swept from 1548 to 1553 nm is shown in Fig. 2(b), which is nearly a perfect sinc² profile for ideal phase matching. Nevertheless, the presence of parasitic phase matching peaks is primarily due to fabrication imperfection and uniformity of the LN layer [16]. The main QPM peak is centered at 1550.6 nm with normalized SHG efficiency of 105% W⁻¹ cm⁻² (100% × output SHG power/[(input fundamental power)² × (waveguide length)²] and full width at half-maximum (FWHM) phase matching bandwidth of 0.8 nm. For OPA applications, a well-defined phase matching profile and high conversion efficiency are crucial for achieving high gain and extended amplification bandwidth whilst minimizing the nonlinear cross talk. The experimental setup is depicted in Fig. 1(b). To mitigate SBS in optical fibers and avoiding potential photorefraction damage of the PPLN waveguide, both pump and signal are 10 MHz pulse trains with 130 ps FWHM, created by modulating a wavelength-tunable, narrowlinewidth (≈100 KHz) CW laser using an electro-optical modulator (EOM). The pump wavelength is fixed at 1550.6 nm while the signal wavelength is tunable between 1495 and 1609 nm. We amplify the pump pulses by using a two-stage EDFA system followed by two cascaded DWDM filters to efficiently suppress the amplified spontaneous emission (ASE) by more than 120 dB. The pump and signal pulses are temporally aligned and independently polarization controlled, before being combined into the fiber collimator through a DWDM. The optical pulses are coupled into and out from the waveguide by using a pair of aspheric lenses with coupling ≈1.1 dB, which can be further reduced by correcting the PPLN's asymmetrical transverse mode using cylindrical lens. The propagation loss is ≤ 0.1 dB per cm, which benefits from the shallow etching that reduces scattering loss. The collimated output of the PPLN is guided through a dichroic mirror to separate the SH and telecom wavelength waves. The signal, idler, and pump pulses are coupled into a fiber collimator for subsequent gain and wavelength conversion measurement using an optical spectrum analyzer (OSA). A DWDM is used as a notch filter (with 20 dB rejection ratio) to separate the residual pump from saturating the OSA.

The signal amplification is recorded from 1495 to 1609 nm (limited by the tunable wavelength range of the laser) with various pump peak power. Figure 3(a) shows a typical result for signal pulses at 1608.8 nm and its conjugate idler pulses at 1495.5 nm for two pump power levels. The parametric gain of the signal pulses is measured by comparing its power with and without the pump. The generated idler beam is also observed in Fig. 3(a) at a power level similar to the amplified signal (within ± 0.2 dB). Figure 3(b) shows the pump-powerdependent OPA gain, where for pump peak power of 30, 35, and 41 dBm, the maximum gain is 15.4, 25.6, and 38.3 dB, respectively. The noise floor of the OPA also increases with higher pump power. Yet, with 38.3 dB signal gain, an impressive optical signal-to-noise (OSNR) greater than 43 dB is obtained, which is comparable to similarly broadband hybrid EDFA/Raman amplifier [17]. The measured signal gain values at different wavelengths with various pump peak power is plotted in Fig. 4(a). As seen, with low pump power,

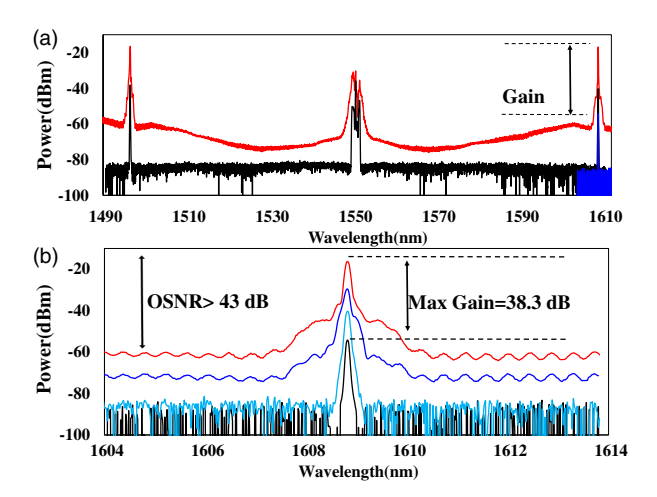


Fig. 3. (a) Typical parametric gain and wavelength conversion spectrum of the PPLN in a cSHG-DFG configuration with 41 dBm (red) and 30 dBm (black) pump peak power. The blue line indicates the input signal spectrum without pump. (b) Amplified signal spectrum with (red) 41 dBm, (blue) 35 dBm, and (cyan) 30 dBm of pump peak power with (black) input signal.

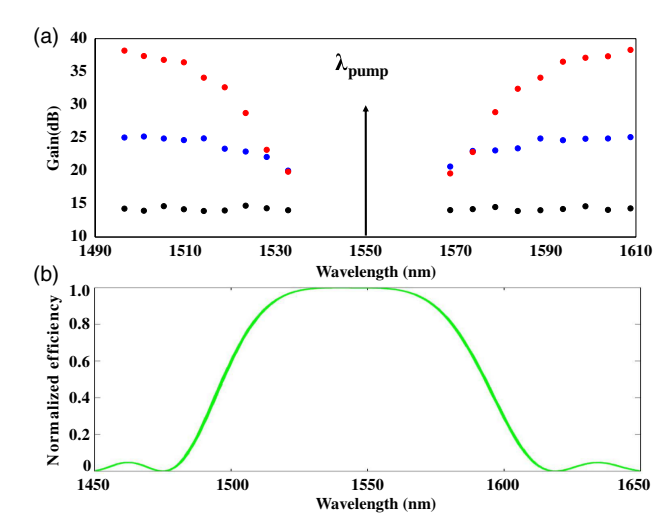


Fig. 4. (a) Measured signal gain as a function of the wavelength with (red) 41 dBm, (blue) 35 dBm, and (black) 30 dBm of pump peak power; (b) theoretical plot of DFG bandwidth.

a reasonably uniform 15 dB gain is achieved over the entire measured wavelength range. In contrast to the theoretical curve of DFG bandwidth shown in Fig. 4(b), at high pump power, we notice that the gain decreases as the signal wavelength edges toward smaller detuning with respect to the pump wavelength. The discrepancy between the theoretical prediction and measured gain profile maybe limited by the fabrication tolerance of the PPLN waveguide, such as the material inhomogeneity and stitching errors [16,18]. Tolerances in fabrication, especially the electric field poling process, may result in distribution of QPM periods, allowing for a broader DFG bandwidth [18,19] and a wider-than-expected gain profile measurement.

Attempting to understand the underlying physics of the competing nonlinear processes that might contribute to starkly different gain profiles, we measure the SH spectrum at a high pump power of 41 dBm. The result is shown in Fig. 5(a). Accompanying the SHG of the pump at 775.3 nm, secondary peaks appear at 779.7 and 770.8 nm. This is because the strong signal (idler) undergoes SFG with the pump, via $1550.6 + 1568.5 \text{ nm}(1533.1 \text{ nm}) \Rightarrow 779.7 \text{ nm}(770.8 \text{ nm})$,

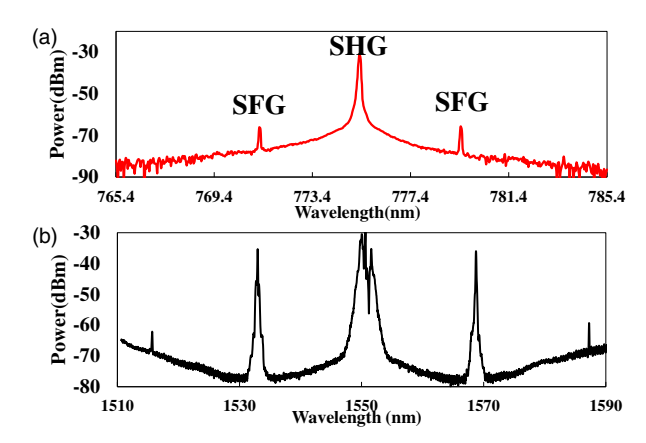


Fig. 5. (a) Measured SH and SF generation with 41 dBm of pump peak power. (b) Observed additional conjugate peaks due the generated SF.

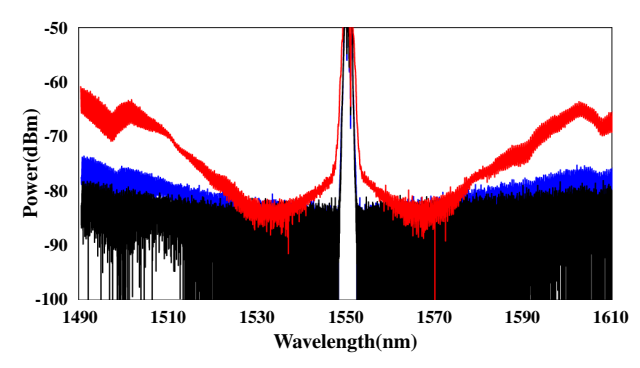


Fig. 6. Amplified quantum noise with (red) 40 dBm, (blue) 20 dBm, and (black) 10 dBm of pump peak power.

as permitted by parasitic phase matching peaks shown in Fig. 2(b). The reduced gain at smaller detuning is thus due to the significant nonlinear crosstalk by the virtue of SFG between the pump and signal and idler pulses. Furthermore, parasitic peaks also allow the SF generated by the pump and signal (idler) to interact with the idler (signal), thus creating corresponding phase conjugated peaks at 1516.0 and 1586.6 nm, as shown in Fig. 5(b). This highlights the importance of well-tailored and narrowband phase matching bandwidth to eliminate the parasitic phase matching peaks. Therefore, recently demonstrated two-stage SHG-OPA [20] presents a solution to alleviate the nonlinear cross talk with high-gain OPA.

To determine the origin of the noise floor of the OPA, we remove the signal pulses and add two free-space optical bandpass filters (center wavelength: 1550 nm, FWHM: 12 nm) with 140 dB extinction right before the input coupler of the PPLN waveguide. The measured OPA noise spectrum is shown in Fig. 6. The noise level is proportional to the pump power and unevenly distributed over the entire S, C, and L bands. With lower pump power, the OPA's noise floor is very low and relatively flat over the entire spectrum. As the pump power increases, the noise floor started to increase significantly and become nonuniform. As the ASE noise from the EDFA and the Raman scattering noise from the subsequent optical fiber is well rejected before the waveguide, the observed noise spectrum must be created intrinsically in the waveguide. It could primarily attribute to scattering-initiated parametric noise [21] or amplified spontaneous parametric down conversion (SPDC) of strong SH pulses in the waveguide, both of which share the identical phase matching condition with the DFG [22]. However, the spectral distribution of the noise is not understood yet and subject to further studies. Further theoretical and experimental investigations are needed to fully understand the physical origin of the noise and gain profile of the OPA [23]. The measured noise floor of the OPA is analogues to the noise floor of the EDFA due to ASE but can be further reduced by operating the OPA in phase-sensitive operations [20], which can further improve the OSNR.

In summary, we have demonstrated efficient parametric amplification over a wide spectrum, covering S, C, and L telecom bands by using a cSHG-DFG configuration. Using an optimally mode-matched PPLN, we achieve maximum parametric gain as high as 38.3 dB and amplification bandwidth over 14 THz. Furthermore, we measure the noise floor and

identify the origin of undesirable competing nonlinear processes, which can be suppressed by well-tailored phase-matching engineering [24]. Nonetheless, implementing the PPLN-based OPA with a CW pump remains challenging due to the undesirable phenomena at high average power including photorefraction effect, domain reversal, green-induced infrared absorption, and light-induced heating. Our results suggest that this cascaded realization of OPA can be used as wideband amplifiers for large capacity optical communications and high-speed all-optical signal processing.

Funding. Office of Naval Research (ONR) (N00014-15-1-2393); National Science Foundation (NSF) (EFRI-1641094).

Acknowledgment. We acknowledge HC Photonics for technical support.

REFERENCES

- E. Agrell, M. Karlsson, A. R. Chraplyvy, D. J. Richardson, P. M. Krummrich, P. Winzer, K. Roberts, J. K. Fischer, S. J. Savory, B. J. Eggleton, M. Secondini, F. R. Kschischang, A. Lord, J. Prat, I. Tomkos, J. E. Bowers, S. Srinivasan, M. Brandt-Pearce, and N. Gisin, J. Opt. 18, 063002 (2016).
- A. D. Ellis, N. M. Suibhne, D. Saad, and D. N. Payne, Philos. Trans. R. Soc., A 374, 2062 (2016).
- J. M. Kahn and K.-P. Ho, IEEE J. Sel. Top. Quantum Electron. 10, 259 (2004).
- A. E. Willner, S. Khaleghi, M. R. Chitgarha, and O. F. Yilmaz, J. Lightwave Technol. 32, 660 (2014).
- R. G. H. van Uden, R. A. Correa, E. A. Lopez, F. M. Huijskens, C. Xia, G. Li, A. Schülzgen, H. de Waardt, A. M. J. Koonen, and C. M. Okonkwo, Nat. Photonics 8, 865 (2014).
- 6. J. Pedro and N. Costa, J. Lightwave Technol. 36, 1552 (2018).
- 7. G. K. P. Lei and M. E. Marhic, Opt. Express 22, 8726 (2014).
- M. E. Marhic, P. A. Andrekson, P. Petropoulos, S. Radic, C. Peucheret, and M. Jazayerifar, Laser Photon. Rev. 9, 50 (2015).
- T. Kishimoto, K. Inafune, Y. Ogawa, N. Sekine, H. Murai, and H. Sasaki, Optical Fiber Communication Conference (2017) paper W2A.12.
- T. Kishimoto, K. Inafune, Y. Ogawa, H. Sasaki, and H. Murai, Opt. Lett. 41, 1905 (2016).
- T. Umeki, T. Kazama, O. Tadanaga, K. Enbutsu, M. Asobe, Y. Miyamoto, and H. Takenouchi, J. Lightwave Technol. 33, 1326 (2015)
- X. Guo, N. Liu, Y. Liu, X. Li, and Z. Y. Ou, Opt. Lett. 41, 653 (2016).
- T. Kishimoto, K. Inafune, Y. Ogawa, N. Sekine, H. Murai, and H. Sasaki, Proc. SPIE 10535, 105350B (2018).
- 14. U. Schlarb and K. Betzler, Phys. Rev. B 48, 15613 (1993).
- 15. H. Ishikawa and T. Kondo, Appl. Phys. Express 2, 042202 (2009).
- 16. R. Nouroozi, J. Lightwave Technol. 35, 1693 (2017).
- J. R. F. de Oliveira, U. C. de Moura, G. E. R. de Paiva, A. P. de Freitas, L. H. H. de Carvalho, V. E. Parahyba, J. C. R. F. de Oliveira, and M. A. Romero, J. Lightwave Technol. 31, 2799 (2013).
- M. Neradovskiy, E. Neradovskaia, D. Chezganov, E. Vlasov, V. Y. Shur, H. Tronche, F. Doutre, G. Ayenew, P. Baldi, M. D. Micheli, and C. Montes, J. Opt. Soc. Am. B 35, 331 (2018).
- A. Tehranchi and R. Kashyap, J. Lightwave Technol. 26, 343 (2008).
- T. Kazama, T. Umeki, M. Abe, K. Enbutsu, Y. Miyamoto, and H. Takenouchi, J. Lightwave Technol. 35, 755 (2017).
- J. Wang, J. Ma, P. Yuan, D. Tang, B. Zhou, G. Xie, and L. Qian, Opt. Lett. 40, 3396 (2015).
- 22. M. Liscidini and J. E. Sipe, Phys. Rev. Lett. 111, 193602 (2013).
- Z. Tong, A. Bogris, C. Lundström, C. J. McKinstrie, M. Vasilyev, M. Karlsson, and P. A. Andrekson, Opt. Express 18, 14820 (2010).
- 24. D. T. Reid, J. Opt. A 5, S97 (2003).